Energy & Environmental Science

Cite this: *Energy Environ. Sci.*, 2011, **4**, 2567

www.rsc.org/ees

PAPER

Highly efficient smart photovoltachromic devices with tailored electrolyte composition

Alessandro Cannavale,[a] Michele Manca,*[a] Francesco Malara,[b] Luisa De Marco,[a] Roberto Cingolani[a] and Giuseppe Gigli[b]

Received 25th February 2011, Accepted 15th April 2011
DOI: 10.1039/c1ee01231b

Driven by the tremendous opportunities offered by dye solar cells technology in terms of building integration, a new generation of smart multifunctional photoelectrochemical cells has the potential to attract the interest of a rapidly growing number of research institutions and industrial companies. Photovoltachromic devices are capable to produce a smart modulation of the optical transmittance and, at the same time, to generate electrical power by means of solar energy conversion. In this work, a specifically designed bifunctional counterelectrode has been realized by depositing a C-shaped platinum frame which bounds a square region occupied by a tungsten oxide (WO_3) film onto a transparent conductive substrate. These two regions have been electrically separated to make possible distinct operations on one or both of the available circuits. Such an unconventional counterelectrode makes it possible to achieve a twofold outcome: a smart and fast-responsive control of the optical transmittance and a relatively high photovoltaic conversion efficiency. In particular we investigated the effect of the electrolyte composition on both photoelectrochromic and photovoltaic performances of such devices by systematically tuning the iodide content in the electrolyte. The best result was obtained by filling the cell with an iodine concentration of 0.005 M: a coloration efficiency of 61.10 $cm^2\ C^{-1}$ at a wavelength of 780 nm and, at the same time, a photovoltaic conversion efficiency of 6.55% have been reported.

1 Introduction

Interest in "smart" materials and devices has exponentially increased in recent years as a direct consequence of the considerable achievements attained in the emerging field of nanotechnologies. "Smart" devices can react to external stimuli by modifying their behaviour in response to the variation of some specific external condition.[1] As an example, an electrochromic (EC) device is characterized by the ability to sustain reversible

[a]*Center for Biomolecular Nanotechnologies (CBN) of Italian Institute of Technology (IIT), Via Barsanti 1, Arnesano, 73010, Italy. E-mail: michele.manca@iit.it; Tel: +39 0832 295739*
[b]*NNL, National Nanotechnology Laboratory of CNR, Istituto di Nanoscienze, Distretto Tecnologico, Università del Salento, Via Arnesano 16, Lecce, 73100, Italy*

Broader context

Recent advances in the field of photoelectrochemistry have produced technologies for liquid-junction solar cells that could potentially compete with solid-state semiconductor photovoltaic technologies. Dye-sensitized solar cells have in fact attracted worldwide both academic and industrial interest due to their advantages in solar energy conversion: these devices are in fact low cost, easily fabricated, environmentally benign and are characterized by a relatively high energy conversion efficiency. One of the main targets of the ongoing research activities consists in the development of innovative concepts for the implementation of photoelectrochemical multifunctional devices capable to integrate two compatible working principles in a single device. A strategic issue in this challenge is represented by the integration of photovoltaic and photoelectrochromic functionalities within a single cell, namely a photovoltachromic cell. This would be a key point in the perspective of building integration, because the photoelectrochromic feature would perform a "control" of undesired solar gains through glazing. A photovoltachromic cell may potentially act as a complex artificial skin, by generating electric energy as a photovoltaic system but also "perceiving" even small variations in external radiation and controlling the energy fluxes by means of a smart variation of their optical transmittance.

and persistent changes of the optical properties when a voltage is applied.[2–4] Electrochromism is an active area for both basic and applied research,[5] due to the potentially huge industrial applications in the field of automotive, aerospace and, most of all, constructions. This is because it has been realised that an EC window has significant energy benefits compared to conventional shading and solar control devices, such as the reduction of cooling, heating and ventilation loads, as well as the ability to replace, at a considerable part, the use of artificial electric lighting by managing daylight admittance.[6]

The electrochromic phenomenon was originally discovered in thin films of tungsten oxide,[7] which still remains the most promising electrochromic material for cathodic coloration, giving an intense Prussian blue in the coloured state and fading to transparence in the bleached state, reversibly. Coloration is due to simultaneous insertion into the tungsten oxide layer of small cations like H^+ or Li^+ and charge balancing electrons into its conduction band through an external circuit. Several theoretical models have been proposed so far, with the aim to ultimately define the physical basis of such electrically driven optical transitions. The most widely accepted models are based on the assumption that electrochromism in tungsten oxide films can be associated to the following mechanisms: (i) intervalence charge transfer (IVCT),[8] (ii) polaronic absorption,[9,10] and (iii) electron trapping by oxygen vacancies.[11] Nevertheless, all these models are singularly unable to explain—thoroughly—the coloration phenomena.

Since the late 1980s several important glass companies have been investing in research on EC materials and devices driven from the perspective to realize effective smart switchable windows capable to sensitively improve the energy efficiency of glass-based building envelopes by reducing demand for space cooling and air conditioning, as well as to positively impact on the indoor comfort,[12,13] thanks to the variable throughput of solar energy and, in particular, visible light.[14]

In 1991 the seminal paper by O'Regan and Graetzel[15] on dye-sensitized solar cells (DSSCs) opened up the possibility to the use of devices based on molecular components for the construction of robust large-scale solar electricity production facilities. DSSCs still represent to date the most suited candidate for the next generation of building integrated photovoltaics.[16]

A dye solar cell consists of a monolayer of photosensitizing dye adsorbed on a mesoporous film of nanocrystalline oxide semiconductor, typically anatase titanium dioxide. Dye molecules are chemisorbed through functional anchoring groups on the surface of the semiconductor, while the pores of the film are generally filled with an iodide/tri-iodide electrolyte.

In 1996 Bechinger *et al.*[17] combined an EC film with a dye-sensitized solar cell electrode to produce what is today known as a photoelectrochromic (PEC thereafter) cell that is an electrochemical cell consisting of two electrodes separated by a redox electrolyte, an electrochromic and a dye-sensitized photovoltaic one, the latter powering the coloration of the former, in response to the incoming solar radiation. In this case, rather than combining an essentially complete photovoltaic cell with a complete EC cell, it was possible to combine just one-half of a typical DSSC with one half of a typical EC cell. In this configuration, the photovoltage produced by the dye sensitized electrode drives electrons and compensates Li^+ cations into the WO_3 film, resulting in a coloured EC film. The coloration process is equivalent to charging a battery: the photovoltage generated by the dye-sensitized electrode is used to charge the EC layer.

The natural technological evolution of the aforementioned road-map should be represented by and integrated photovoltaic-powered (PV–EC) window, considering in particular that the operational characteristics of both PV and EC technologies are highly compatible. A small area of PV cells could in fact provide sufficient electric power to operate a large-area EC window. In spite of these considerations, during the last ten years just a couple of design options have been explored in this contest.[18–20]

First demonstration of a reliable approach to conveniently integrate PV and PEC technologies has been reported only in 2009 by Wu *et al.*[21,22] They developed a novel class of photoelectrochemical devices, namely photovoltachromic cells (PVCCs), capable to exhibit a fair photoelectrochromic behaviour that is to modulate their optical transmittance with no need of external energy supply, and, simultaneously, to produce electrical power by photovoltaic conversion, since they can work exactly as DSSCs. Energy conversion efficiency exhibited by this first PVCC was about 0.5% and it was not possible to manage PV and PEC functionalities separately. Starting from these remarks, we investigated the key mechanisms laying on the basis of the working principle of these bifunctional devices and focused on the pivotal role played by the iodine/iodide-based electron mediator. To this aim the electrolyte composition has been systematically modified by tuning the molar ratio $[I^-]/[I_3^-]$ and the effect of two commonly used additives has also been evaluated.

We finally realized an optimized PVCC capable to show a significant enhancement of the photovoltaic performances with respect to the state of art, as well as a remarkable improvement of the coloration kinetics resulting in the reduction of the response time in both colouring and bleaching processes.

2 Discussion of results

2.1 Morphological and optical properties of the electron beam evaporated WO_3 layers

Electrochromic WO_3 layers were contemporaneously deposited by electron beam evaporation onto ITO-coated glass and miscut-Si substrates for XRD characterization. Having tested several deposition conditions (by systematically tuning vacuum pressure, oxygen flux, evaporation rate and substrate temperature) with the aim to optimize the morphological structure of the films, we opted to fix the evaporation rate at 1.5 Å s^{-1} and the oxygen flux at 20 sccm: deposition processes taking place in the presence of an oxygen flux allow a significant increase of roughness of the tungsten oxide film.[23] Extended surface roughness and high porosity are two fundamental requirements to achieve optimal electrochromic performances,[24,25] since they strongly impact the value of the lithium diffusion constant into the WO_3, which typically varies from 1.5×10^{-12} to 5×10^{-9} cm^2 s^{-1}, depending on the shape and number of pathways available for cations intercalation.[26]

Besides, substrate temperature throughout the deposition process significantly affects the optical properties of the film, in

particular its crystalline phase: an amorphous tungsten oxide film can be obtained at temperatures lower than 350 °C, whereas crystalline features start to appear at higher temperatures.[27] We thus opted to work at a temperature of 230 °C in order to obtain a highly disordered amorphous phase that, as it is well known,[28] allows to achieve a larger transmittance modulation within the visible spectrum. Fig. 1 shows a typical diffraction pattern collected from either a 200 nm or 300 nm thick WO_3 layer deposited by e-beam at 230 °C. The absence of sharp diffraction peaks in these patterns is indicative of the lack of a long range order. The only broad noticeable peak is indicative of monoclinic WO_3 which appears above 100 °C at around 23.1°, indicating the presence of very small nanoparticles[29] The two broad diffraction maxima indicate the presence of very small crystallites in the short range order. The broadness of diffraction peaks in other positions suggests that crystalline and amorphous phase coexist. A direct comparison with the expected diffraction pattern of amorphous tungsten oxide already observed in the literature[30] confirms this assumption.

As visible in Fig. 2, scanning electron microscopy (SEM) analysis revealed a nonporous structure characterized by a quasi-ordered arrangement of nanometric clusters that is responsible for a reasonably fair surface roughness (RMS 2–3 nm).

Optical transmittance modulation for three different tungsten oxide layers having respectively 150 nm, 200 nm and 300 nm thickness was measured in the wavelength range between 250 and 2500 nm by implementing conventional photoelectrochromic cells (PECCs).[17] Transmittance spectra of either bleached (as prepared) or coloured (10 min illumination at 1.5 AM under 100 mW cm^{-2}) PECCs are reported in Fig. 3. In the bleached state substantially no differences were observed in the maximum transmittance of the three layers, although thicker ones showed slightly longer UV cut-off wavelengths. In the coloured state, the thickest WO_3 layer (300 nm) exhibited the widest transmittance modulation as a consequence of its greatest volume of pathways available for the insertion of lithium cations. This characteristic dependence of ΔT on the film thickness has been previously demonstrated to be consistent with the variation of the optical density of the electrochromic layers.[31]

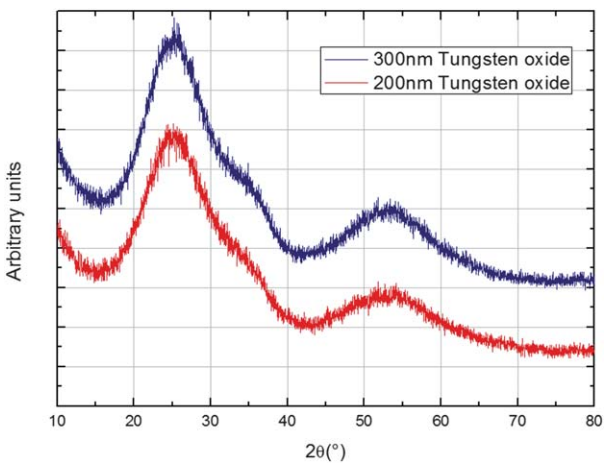

Fig. 1 X-Ray diffraction pattern of two different WO_3 layers deposited by e-beam evaporation at 230 °C.

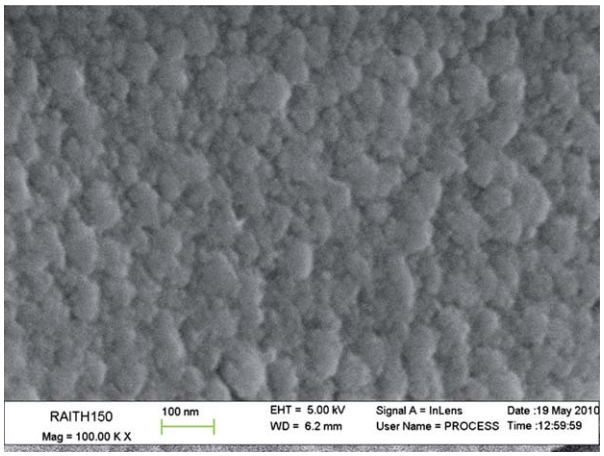

Fig. 2 SEM image showing the surface of a 300 nm thick WO_3 layer deposited by e-beam evaporation at 230 °C.

Optical density is a scalar quantity that can be calculated from the measured spectral transmittance according to the following expression:[32]

$$\Delta OD = \log\left(\frac{T_{Ble}^{Vis}}{T_{Col}^{Vis}}\right) \quad (1)$$

where T_{ble} and T_{col} are—respectively—the transmittance in the bleached and in the coloured state.

An as high ΔOD as 0.83 was thus observed at 780 nm in the case of PECCs employing a 300 nm thick WO_3 layer (0.68 at 425 nm). Thus we opted to use 300 nm thick tungsten oxide layers for the fabrication of the photovoltachromic devices investigated in the present study.

2.2 Intelligent bi-functional frame-type counterelectrodes

The above described 300 nm thick EB-deposited WO_3 layer was thus used to fabricate both conventional photoelectrochromic cells[17] and innovative frame-type photovoltachromic cells

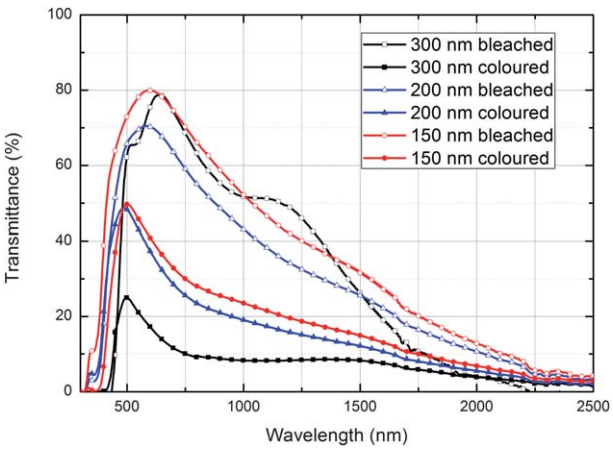

Fig. 3 Transmittance spectra of PECCs based on three different WO_3 thicknesses in the as-prepared and the colored states, measured in open circuit conditions.

(PVCCs) implementing a patterned bifunctional counter-electrode. Such a counterelectrode was constituted by a C-shaped platinum frame that surrounded a square 25 mm^2 WO_3 region (see Experimental details). On the conductive side of the front-on glass a C-shaped photoelectrode was realized in a such way as to be perfectly superimposable to the facing platinum frame. Then, catalyst and electrochromic regions were electrically separated by means of a diamond scriber in order to make distinct operations possible on one or both of the available circuits.

This allowed the measurement of two different sets of parameters: those corresponding to the photovoltaic functionality (PV circuit) and those corresponding to the photoelectrochromic one (PEC circuit). The device disclosed here allows various switching modes. It colours under illumination in short circuit conditions and bleaches in the dark. A schematic representation of our frame-type PVCCs is reported in Scheme 1.

In order to exploit the best compromise between coloration kinetics and photovoltaic performances, six different electrolytes were designed and tested either in conventional PECCs or in our frame-type PVCCs. In Table 1 the chemical composition of the six employed electrolytes is reported (in all the cases acetonitrile has been used as solvent): we opted to tune the iodine concentration and then to evaluate the effect of some conventional additives while keeping constant the lithium iodide concentration. It is well known, in fact, that the concentration of I_3^- in the electrolyte dominates the performance of the DSSC and that, for sufficient amount of I^- and cations, the concentration of I^- does not affect the performances of the cell.[33,37] For this reason, we chose to fix a 0.7 M content of lithium iodide in all the tested electrolytes.

2.3 Effect of the electrolyte composition on the coloration kinetics

As a first experimental evidence we observed that the presence of the platinum layer on the counterelectrode led to a hugely faster switchability of the electrochromic layer state with respect to the corresponding PECCs in both bleaching and coloring processes. Platinum is in fact responsible of a twofold task: it catalyzes the regeneration of I^- species and, at the same time, promotes the electron transfer from WO_3 to the electrolyte, thus accelerating the photoelectrochromic processes. This reaction does not take place in a PECC, where bleaching is only possible in two ways: electrons flow back *via* the external circuit (switch closed) or by loss reactions.[4]

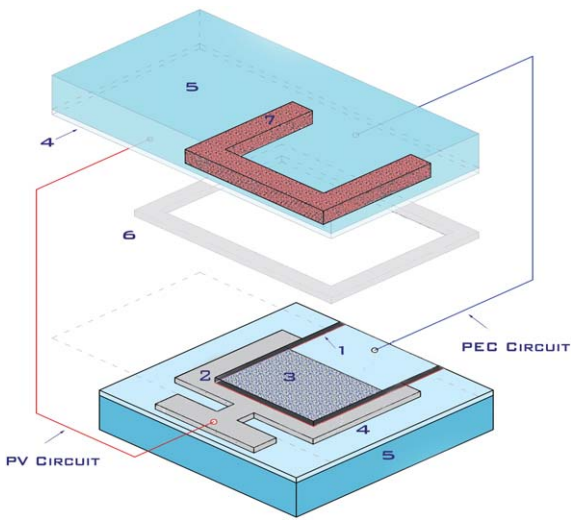

Scheme 1 Schematic representation of the photovoltachromic cells realized for the present study. (1) Electric separation on the counter-electrode; (2) platinum catalyzer; (3) tungsten oxide layer; (4) TCO; (5) glass substrate; (6) sealant; (7) titanium dioxide and dye absorbed; circuitry: red: photovoltaic; blue: photoelectrochromic.

In our considerations, colouring time t_c and bleaching time t_b are defined, respectively, as the time required to achieve a transmittance change equal to two-thirds of the difference between the steady-state transmittances in bleached and coloured states.[21]

Concerning the impact of the electrolyte on the photoelectrochromic behaviour of our PVCCs, a significantly faster switchability was revealed when the iodine content in the electrolyte was reduced from 0.05 M to 0.005 M (see (Table 1)): the colouring time passed in fact from 15 s to 6 s and the bleaching time from more than one minute to 15 s. A further reduction of the iodine concentration down to 0.0025 M did not turn into faster colouring/bleaching response times. Furthermore, we decided to investigate the effect of the addition of two conventional additives with the aim to increase the open circuit voltage: we observed how the addition of either 0.5 M of *tert*-butylpyridine (4-TBP) or 0.1 M of guanidinium thiocyanate (GNDT) to EL3 produced noticeable variations in the response kinetics. Colouring in devices employing EL5 was further reduced down to 5 s. Then, aiming to quantitatively evaluate the effect of tuning the electrolyte composition, we measured the coloration efficiency (CE) that is a convenient parameter to characterize PVCCs in terms of electrochromism.[34] CE is defined by:

$$CE = \frac{\Delta OD}{\Delta Q} \quad (2)$$

where ΔOD is the change in the optical density associated to the coloration of the WO_3 film and ΔQ is the charge exchange effecting such ΔOD. Fig. 4 shows the spectral coloration efficiency of PVCCs filled with the six different electrolytes referred above. The shape of all the curves is obviously determined by the optical transmittance modulation of the electron beam evaporated tungsten oxide film and CE tends to be a maximum in the near infrared region, as previously reported by Ozkan *et al.*[27] Electrolytes EL3 and EL5 showed the best CEs: EL3-based PVCC showed a value of 53.46 cm^2 C^{-1} at 780.46 cm^2 C^{-1} at 780 nm whereas EL5 (that has been obtained by adding 0.5 M of TBP to EL3) allowed to further increase this value up to 61.10 cm^2 C^{-1}. The trend previously observed for the response times appeared to be confirmed too: as the iodine concentration was reduced from 0.5 M to 0.005 M the CE resulted in fact enhanced by a factor higher than 3. A picture of the EL5-based cell either in the bleached or in the coloured state is shown in Fig. 5.

The stability of the optical modulation process was also tested by subjecting the cells to alternate cycles of colouring and bleaching by means of the application of low negative and positive bias voltages, respectively. Up to 10^2 cycles were run and no significant reduction of peaks intensity was observed. In the diagram represented in Fig. 6 the modulation of an EL5-based device after 10 cycles is reported. A voltage equal to the photovoltage of the cell was applied (0.75 V). The significant

Table 1 Effect of electrolyte composition on the photoelectrochromic response kinetics

Electrolyte	$[I_2]$/M	[LiI]/M	Additives/M	Redox potential/V	t_c/s PECC	t_b/s PECC	t_c/s PVCC	t_b/s PVCC
EL1	0.05	0.7	—	0.321	>60	≫60	15	>60
EL2	0.025	0.7	—	0.312	40	≫60	10	60
EL3	0.005	0.7	—	0.292	15	>60	6	15
EL4	0.0025	0.7	—	0.283	30	>60	20	25
EL5	0.005	0.7	4-TBP/0.5	0.292	8	>60	5	10
EL6	0.005	0.7	4-TBP/0.5, GNDT/0.1	0.292	9	>60	7	15

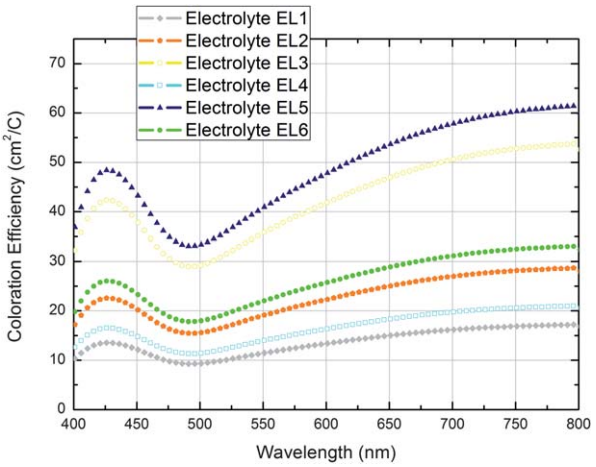

Fig. 4 Coloration efficiency *vs.* wavelength of PVCCs filled with different electrolytes.

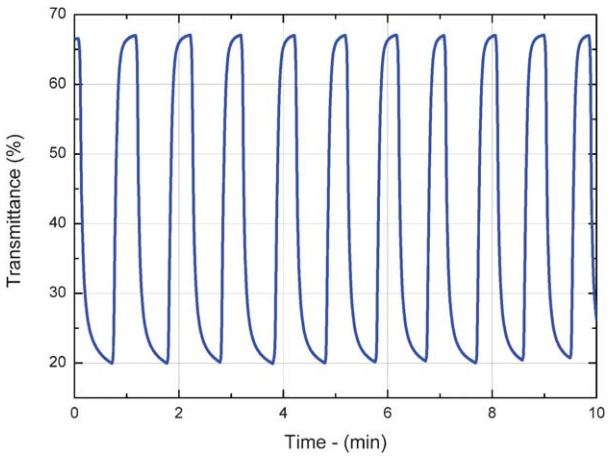

Fig. 6 Cyclic transmittance modulation in a PVCC filled with the electrolyte EL5.

reduction of response times is noticeable in this graph, but also the stability of the peaks through time can be appreciated.

2.4 Effect of the electrolyte composition on the photovoltaic performances

Besides, having short-circuited the PEC cell, we investigated the photovoltaic performances with the aim to assess the influence of the electrolyte formulation on the photovoltaic performances. In Fig. 7 current–voltage (J–V) characteristics of PVCCs measured under AM 1.5 illumination at 100 mW cm^{-2} (Standard Test Conditions—STC) are reported.

A systematic rise in the performances was revealed as the iodine concentration was lowered from 0.05 M to 0.005 M and a photocurrent density of 17.2 mA cm^{-2} was measured for EL3-based PVCCs. V_{oc} resulted also improved when the concentration of I_2 was reduced, as a consequence of a negative shift in the electrolyte redox potential.[35] This trend is well consistent with the findings of Hoshikawa *et al.*[36] who demonstrated that recombination between the injected electrons in TiO_2 and I_3^- constitutes the main limiting factor in conventional iodide/iodine based electrolytes. On the other hand, no limitation in the diffusion coefficient has been ever reported for iodide concentration comprised between 0.1 M and 1 M of Li^+ in liquid electrolyte based-DSSCs.[37]

Fig. 5 Images showing the EL5-based PVCC in the bleached (left) and coloured (right) state respectively.

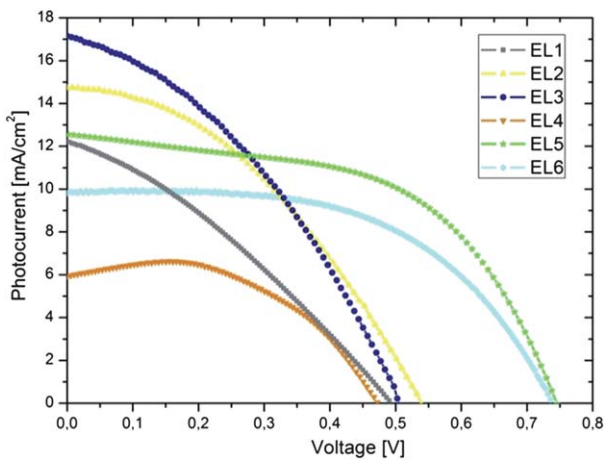

Fig. 7 J–V characteristics of PVCCs filled with different electrolytes.

Nevertheless, a further reduction in the iodine content down to 0.0025 M, as in the EL4-based device, determined a loss of performances ($\eta = 1.94\%$, $J_{sc} = 6.0$ mA cm^{-2}, $V_{oc} = 0.47$ V, FF = 0.69) that can be clearly attributed to the lack of balance between the two redox species. In this case the maximum photocurrent was not revealed at short circuit condition, this clearly attesting the insufficient value of the limiting diffusion current.[36]

Then, aiming to reduce the recombination rate between the injected electrons in TiO_2 and I_3^-, we designed two more specific electrolytes starting from the top-performing one (EL3); two commonly employed stabilizing additives were added to its formulation.

EL5 was prepared by adding 0.5 M of TBP to EL3 solution. This led to a significant increment of both open circuit voltage (0.74 V) and fill factor (0.72) of the device and as high photovoltaic conversion efficiency as 6.65% was measured. TBP is typically added to improve the photovoltaic performances in DSSCs since it gives rise to a negative shift of the TiO_2 conduction band, thus generating an increase of the cell photovoltage.[33]

EL6 was then prepared by adding 0.1 M of GNDT to EL5 solution. EL6-based PVCCs revealed however a slight decay in J_{sc} with respect to EL5, this attesting that for electrolytes with an as low as 0.005 M concentration of iodine, the passivating effect induced by the GNDT adsorption on TiO_2[38] does not turn into a further reduction of the recombination rate if compared with the effect obtained by adding only 0.5 M of TBP.

2.5 How does the photoelectrochromic switching affect the photovoltaic performances?

Then, having interrupted the electrical continuity between the outer platinum frame and the inner tungsten oxide region on the counterelectrode's plate, we performed a systematic investigation of the photovoltaic performances both in the coloured and in the bleached WO_3 state.

We discovered that when the PEC circuit was closed under illumination such as a steady coloration state of the WO_3 layer was reached, a slight increase in the photovoltaic performances could be achieved. This effect was observed for all the six electrolytes tested in this study. Data reported in Table 2 testify such a finding. It reports the photovoltaic performances (J_{sc}, V_{oc}, FF, η) of PVCCs measured both when the PEC circuit is open-circuited and when it is short-circuited.

More in detail, we revealed a significant increase of both J_{sc} and V_{oc} for the case of the EL1–EL4-based cells, whereas additives containing electrolytes (EL5 and EL6) exhibited only a slight enhancement of the J_{sc}.

Such an observed increase in photocurrent density can find a coherent explanation if considering the role played by lithium cations in the building up of an electric double layer (Helmholtz and diffuse layers) at the interface between the dye-sensitized mesoporous photoanode and the electrolyte. Being an adsorptive hard cation, Li^+ can in fact penetrate the space between the adsorbed dye molecules and the surface of TiO_2 and thus screen the negatively charged TiO_2 within the size of the dye.[37] Since the I_3^- concentration profile is determined either by the potential of the TiO_2 or the concentration profile of lithium cations, after the coloration process a huge amount of them[39,40] are confined in the WO_3 and the concentration of I_3^- within the thickness of the electric double layer results reduced. Beside this, positive Li^+ cations, when exorbitant, create deeper trap sites which prevent injected electrons from transferring smoothly in TiO_2, and charge recombination between the injected electrons and I_3^- occurs through these sites.[36] So it is reasonable to suppose that in a PVC device, the coloration process at the counterelectrode turned into a mitigation of the photogenerated charge recombination at the photolectrode/electrolyte interface.

With this regard, it can be useful here to provide some short remarks on the physics of these complex photoelectrochemical systems. Scheme 2 shows an approximated scheme of the energy levels distribution in a PVVC.

It is well known that the top of the WO_3 valance band arises from oxygen p states and the bottom of the conduction band is mainly derived by W5d states with some mixing with oxygen 2p states. So the WO_3 band gap is a sensitive function of W–O bond length. Therefore, in amorphous WO_3 containing oxygen vacancies, as in the case of our electron beam evaporated films, there is a structural relaxation resulting in an increase of W–W distance and changes in W–O splitting.[41] According to the Deb's theory, in fact, such a relaxation induces the presence of a significant number of in-gap energy states (W^{6+}): electronic transitions between W^{6+} states and W^{5+} states, that are localized just below the Fermi level, are then responsible of the color centers formation. Fermi level of the WO_3 film has been represented by two dashed lines to take into account the electrochromic state of the film: E_{fb} and E_{fc} indicate the Fermi level in the bleached and in the coloured state respectively.[12] The relative

Table 2 Photovoltaic parameters and response times in PVCCs filled with different electrolytes

Electrolyte	$[I_2]$/M	[LiI]/M	Additives/M	J_{sc}/mA cm^{-2}	V_{oc}/V	FF	η (%)	WO_3 state (Ble/Col)
EL1	0.05	0.7	—	12.10	0.49	0.55	3.26	Col
				11.19	0.48	0.50	2.68	Ble
EL2	0.025	0.7	—	14.80	0.54	0.60	4.79	Col
				14.05	0.49	0.57	3.92	Ble
EL3	0.005	0.7	—	17.20	0.51	0.58	5.00	Col
				16.18	0.51	0.58	4.78	Ble
EL4	0.0025	0.7	—	9.20	0.50	0.39	1.70	Col
				4.30	0.47	0.56	1.13	Ble
EL5	0.005	0.7	4-TBP/0.5	12.30	0.74	0.72	6.55	Col
				11.59	0.76	0.68	5.99	Ble
EL6	0.005	0.7	4-TBP/0.5, GNDT/0.1	9.90	0.73	0.69	4.98	Col
				9.28	0.76	0.68	4.79	Ble

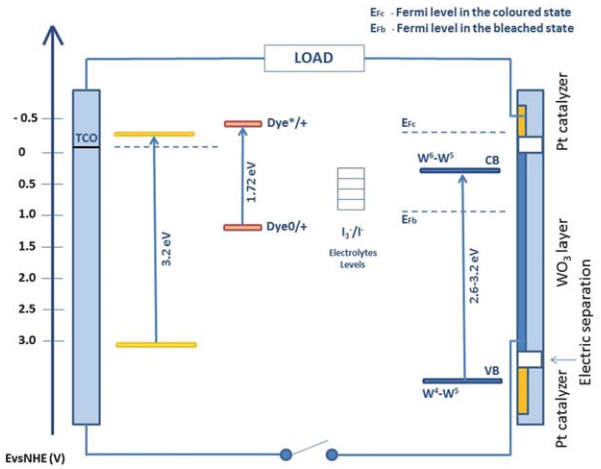

Scheme 2 Schematic representation of the energy levels in a photovoltachromic cell.

position of the Fermi level in the coloured WO_3 with respect to the Fermi level of TiO_2 in the dark plays a pivotal role in determining the responsivity of the bleaching process, whereas the effectiveness of the coloring process is mainly determined by the intensity of the photocurrent available for injection in the WO_3, or, in other words, by the performance of the dye-sensitized photoelectrode.

Moreover, although we did not report it in the present paper, we experimentally verified that even the most performing electrolytes (EL3, EL5 and EL6) did not produce an effective coloration in PVCCs in which no electric separation had been realized between WO_3 and Pt on the counterelectrode; this can be reasonably explained as due to the following: photoelectrons that are injected into the tungsten oxide conduction band are suddenly transferred to the adjacent platinum layer (because of the lower energy position of its Fermi level) and then transferred to the oxidized species in the electrolyte; for this reason, no coloration process can take place. The separation of the two circuits disclosed here allows instead a heavy lithium adsorption on WO_3 and, at the same time, an efficient regeneration of the oxidized electrolytic species. A quantitative analysis of such phenomenon is currently under investigation and will be minutely provided in further reports.

3 Experimental

3.1 Preparation of dye-sensitized photoelectrodes

FTO-coated glasses (20 Ω sq^{-1}, purchased from Kintec) were cleaned in a detergent solution using an ultrasonic bath for 15 min, washed with water and ethanol. A screen-printable paste containing 30 nm sized TiO_2 colloids was prepared according to our previously reported procedure.[42] It was deposited onto the conducting glass by screen-printing (screen characteristic: material, polyester; mesh count, 120 mesh cm^{-1}) through a specifically designed C-shaped mask having an $(8 + 8 + 20) \times 3$ mm^2 aperture and then dried at 160 °C for 6 minutes; this procedure was repeated several times in order to obtain 12 μm thick photoelectrodes. The film thickness and the dimensions of the active area were measured using KLA-TENCOR profilometer. The FTO-glass samples coated with the TiO_2 pastes were gradually heated under an air flow at 160 °C for 20 min, at 325 °C for 5 min, at 375 °C for 5 min, at 450 °C for 15 min, and at 500 °C for 15 min. After cooling to 80 °C, the TiO_2 electrodes were immersed into a 0.5 mM solution of bis(tetrabutylammonium)-*cis*-di(thiocyanato)-*N*,*N*′-bis(4-carboxylato-4′-carboxylic acid-2,2-bipyridine) ruthenium(II) (N719) in a mixture of acetonitrile and *tert*-butyl alcohol (v/v, 1 : 1), and kept at room temperature for 14 h.

3.2 Platinum deposition

Platinum layers were deposited by electron beam deposition (TEMESCAL SUPERSOURCE). The vacuum chamber was initially evacuated to 10^{-7} mbar and then a first 5 nm thick adhesion layer of titanium was deposited. The platinum coating, that had a thickness of 50 nm, was then deposited. The rate of deposition was about 1.0 Å s^{-1} and the e-beam power was about 38%. During the deposition the chamber reached a temperature of about 40 °C.

3.3 Tungsten oxide deposition

Tungsten oxide layers were deposited by electron beam deposition (TEMESCAL SUPERSOURCE). The vacuum chamber was initially evacuated to 10^{-7} mbar and then pure dry oxygen was admitted through a needle valve. The pressure was maintained at 10^{-4} mbar throughout the deposition. The rate of deposition was about 1.5 Å s^{-1} and the temperature was kept constant at 240 °C. X-Ray diffraction (XRD) patterns were collected through an X'PERT PRO Diffractometer (Panalytical), using Cu-Kα radiation supplied with 45 KV and 40 mA. The morphology of the tungsten oxide films has been assessed by Scanning Electron Microscopy (SEM) images performed by a RAITH 150 EBL system. Typically, the images were acquired at 5 kV accelerating voltages using short exposure times. Optical transmittance spectra were observed by a VARIAN 5000 spectrophotometer.

3.4 Cells assembling

The solar cells were assembled by facing the specifically patterned Pt/WO_3 counterelectrode onto the C-shaped dye-sensitized photoelectrode. The two electrodes were assembled into a sandwich type cell and sealed with a Surlyn hot-melt gasket 50 μm thick. The redox electrolyte was introduced into the space of inter-electrodes through the hole pre-drilled on the back of the counter electrode. The holes were sealed up using Surlyn hot-melt film and a cover glass.

3.5 Device characterization

Photocurrent–voltage (*I*–*V*) measurements were performed using a Keithley unit (Model 2400 Source Meter). A Newport AM 1.5 Solar Simulator (Model 91160A equipped with a 300 W Xenon Arc Lamp) served as a light source, and its light intensity (or radiant power) was calibrated to 100 mW cm^{-2} using a reference Si solar cell.

4 Conclusions

We demonstrated a self-powered highly performing dye-sensitized photovoltachromic device characterized by a relatively high photovoltaic energy conversion efficiency and an outperforming smart photoelectrochromic behaviour consisting in a fast switching rate and a widely tunable transmittance under illumination. Thanks to the peculiar architecture of the above referred devices, the balancing of the electrolytic iodine/iodide species turned into a positive outcome on both of their functionalities. So when the iodine concentration was turned from 0.05 M to 0.005 M, not only the photovoltaic performances boosted from 3.26% to 6.55%, but even the coloration efficiency inherent to the smart photochromic behaviour resulted dramatically improved. Moreover, due to the addition of 0.5 M TBP, in the EL5-based device t_b resulted 1/3 with respect to EL3-based ones, in spite they had the same iodine concentration. Such findings allow us to state that EL3 and its derivative EL5 mostly match the electrolyte formulation criteria that optimize the performances of both these functionalities. As a result we strongly believe that the smart and interactive character of devices presented in this study, as well as the prospect of their low-cost fabrication technology, will make them hugely attractive for a wide spectrum of industrial and architectural applications, first of all in the field of building integration with a significant agreement with the UE standards for energy efficiency.[43]

Acknowledgements

This work has been partially supported by Regione PUGLIA (APQ Reti di Laboratorio, Project PHOEBUS, cod. 31). The authors want to thank Paola Pareo for SEM images, Luigi Martiradonna for XRD spectra, Eliana D'Amone for technical support, Francesco Fiorito and Roberto Giannuzzi for beneficial discussions.

Notes and references

1 M. Addington and D. Schodek, *Smart Materials and New Technologies*, Elsevier, Oxford, United Kingdom, 2005.
2 G. C. Granqvist, *Handbook of Inorganic Electrochromic Materials*, Elsevier, Amsterdam, The Netherlands, 2002.
3 B. A. Gregg, *Endeavour*, 1997, **21**(2), 52–55.
4 A. Georg and U. Opara Krasovec, *Thin Solid Films*, 2006, **502**, 246–251.
5 R. Baetens, B. P. Jelle and A. Gustavsen, *Sol. Energy Mater. Sol. Cells*, 2010, **94**(2), 87–105.
6 S. E. Selkowitz, M. Rubin, E. S. Lee, R. Sullivan, E. Finlayson and D. Hopkins, Lawrence Berkeley National Laboratory Report LBL-35486, 1994, pp. 1–23.
7 S. K. Deb, *Appl. Opt., Suppl.*, 1969, **3**, 192–195.
8 B. W. Faughnan, R. S. Crandall and P. M. Heyman, *RCA Rev.*, 1975, **36**, 177.
9 V. Wittwer, O. F. Schirmer and P. Schotter, *Solid State Commun.*, 1978, **25**, 977.
10 E. K. H. Salje, *Eur. J. Solid State Inorg. Chem.*, 1994, **L31**, 805.
11 J. Ritsko, H. Witzke and S. K. Deb, *Solid State Commun.*, 1977, **22**, 455–458.
12 A. Azens and G. C. Granqvist, *J. Solid State Electrochem.*, 2003, **7**, 64–68.
13 S. Leydecker, *Nanomaterials in Architecture, Interior Architecture and Design*, Birkhauser, Berlin, Germany, 2008.
14 T. Herzog, *Solar Chart*, ed. T. Herzog, et al., Prestel Publishing, Berlin, Germany, 2007.
15 B. O'Regan and M. Graetzel, *Nature*, 1991, **353**, 737–740.
16 G. E. Tulloch, *J. Photochem. Photobiol., A*, 2004, **164**, 209–219.
17 C. Bechinger, S. Ferrere, A. Zaban, J. Sprague and B. Gregg, *Nature*, 1996, **383**, 608–610.
18 D. Benson, R. Crandall, S. K. Deb and J. L. Stone, *US Pat.*, 5384653, 1995.
19 S.-H. Lee, W. Gao, C. E. Tracy, H. M. Branz, D. K. Benson and S. K. Deb, *J. Electrochem. Soc.*, 1998, **145**, 3545.
20 G. Tulloch and I. Skryabin, *US Pat.*, 6297900, 2001.
21 J. Wu, M. Hsieh, W. Liao, W. Wu and J. Chen, *ACS Nano*, 2009, **8**, 2297–2303.
22 W. Wu, W. Liao, L. Chen, J. Chen and J. Wu, *Phys. Chem. Chem. Phys.*, 2009, **11**, 9751–9758.
23 G. C. Granqvist, *Handbook of Inorganic Electrochromic Materials*, Elsevier, Amsterdam, The Netherlands, 2002.
24 G. C. Granqvist, *Electrochim. Acta*, 1999, **24**, 3005–3015.
25 K. D. Lee, *Sol. Energy Mater. Sol. Cells*, 1999, **57**, 21–30.
26 G. Niklasson and G. C. Granqvist, *J. Mater. Chem.*, 2007, **17**, 127–156.
27 E. Ozkan, S. Lee, C. E. Tracy, J. R. Pitts and S. K. Deb, *Sol. Energy Mater. Sol. Cells*, 2003, **79**, 439–448.
28 H. Kamal, A. A. Akl and K. Abdel-hady, *Physica B*, 2004, **349**, 192–205.
29 R. S. Vemuri, K. Kamala Bharathi, S. K. Gullapalli and C. V. Ramana, *ACS Appl. Mater. Interfaces*, 2010, **2**(9), 2623–2628.
30 Y. Liu, H. Shen, W. Chen, H. Wang, Y. Deng and D. Wang, *Chin. Sci. Bull.*, 2008, **53**(20), 3173–3177.
31 M. S. Burdis, J. R. Siddle, R. A. Batchelor and J. M. Gallego, *Proc. Soc. Photo-Opt. Instrum. Eng.*, 1995, **2531**, 11.
32 W. J. Lee, Y. K. Fang, J. Ho, W. T. Hsieh, S. F. Ting, D. Huang and F. C. Ho, *J. Electron. Mater.*, 2009, **29**, 183–187.
33 G. Boschloo and A. Hagfeldt, *Acc. Chem. Res.*, 2009, **42**(11), 1819–1826.
34 G. C. Granqvist, *Sol. Energy Mater. Sol. Cells*, 2000, **60**, 201–262.
35 M. K. Nazeeruddin, A. Kay, I. Rodicio, R. Humphry-Baker, E. Muller, P. Liska, N. Vlachopoulos and M. Gratzel, *J. Am. Chem. Soc.*, 1993, **115**, 6382–6390.
36 T. Hoshikawa, T. Ikebe, R. Kikuchi and K. Eguchi, *Electrochim. Acta*, 2006, **51**, 5286–5294.
37 S. Nakade, T. Kanzaki, W. Kubo, T. Kitamura, Y. Wada and S. Yanagida, *J. Phys. Chem. B*, 2005, **109**, 3480–3487.
38 N. Kopidakis, N. R. Neale and A. J. Frank, *J. Phys. Chem. B*, 2006, **110**, 12485–12489.
39 H. Morita, *Jpn. J. Appl. Phys.*, 1985, **6**, 750–754.
40 J. G. Zhang, D. K. Benson, C. E. Tracy, S. K. Deb, A. W. Czanderna, C. Bechinger, *presented at 190th Electrochemical Society Meeting, San Antonio, Texas*, October 1996.
41 S. K. Deb, *Sol. Energy Mater. Sol. Cells*, 2008, **92**, 245–258.
42 L. De Marco, M. Manca, R. Giannuzzi, F. Malara, G. Melcarne, G. Ciccarella, I. Zama, R. Cingolani and G. Gigli, *J. Phys. Chem. C*, 2010, **114**, 4228–4236.
43 Directive 2002/91/EC, Directive 2002/91/EC of the European Parliament and of the council of 16 December 2002 on the energy performance of buildings, *Official Journal of the European Communities*, 4 January 2003, OJ L 1/65.

